Performance Verification and Testing of the COWVR Instrument Antenna

Paolo Focardi, David González-Ovejero, Jefferson A. Harrell and Shannon T. Brown
Jet Propulsion Laboratory, California Institute of Technology, Pasadena, CA 91109 USA

***Abstract*— The Compact Ocean Wind Vector Radiometer (COWVR) is a technology demonstration mission, developed at the Jet Propulsion Laboratory (JPL), and scheduled for launch in 2016. The goal of COWVR is to provide the same wind vector retrieval accuracy of other instruments, like WindSat, while reducing the total mass and using less power. In this paper, we present an overview of the COWVR instrument, and a detailed description of the EM modeling of the antenna system and the test campaign carried out at JPL to assess its performance. Special emphasis has been placed on assessing the accuracy of the predictions made with the RF model. We will show that the predicted radiation patterns are accurate enough so one can use them for orbit radiometer calibration.**

***Index Terms*—reflector antenna, horn antenna, off-set reflector, radiometer, scanning antenna, anechoic chamber measurements, radiation patterns.**

I. Introduction

The Compact Ocean Wind Vector Radiometer (COWVR) mission has been developed at Jet Propulsion Laboratory (JPL), in collaboration with the US Air Force Space and Missile Systems Center. COWVR has been conceived as a proof of concept mission and it is scheduled for launch in 2016. The technology to be demonstrated is a low-cost, low-mass, low-power, fully-polarimetric imaging radiometer in the K and Ka bands. First, the reduced size of the instrument is well adapted for implementation on an ESPA-class satellite, enabling a low-cost launch as a secondary payload. More importantly, the fully-polarimetric capability enables the retrieval of the ocean surface wind vector, along with other key environmental parameters, namely, precipitable water vapor, cloud liquid water, precipitation rate and sea ice. The novel design adopted for COWVR has allowed us to reduce the system complexity which in turn significantly reduces the cost, mass, power and volume from the heritage WindSat sensor [1]. Yet, is predicted to maintain the same wind vector retrieval accuracy.

II. Antenna System and RF Model

In the following, we will focus on the instrument's antenna; the reader is referred to [2] for a detailed description of the radiometer and its capabilities. The antenna system consists of an offset-fed reflector with a 75cm diameter parabolic dish and focal length equal to 43cm. The feed's phase center is placed at the focus of the reflector with no edge offset. Hence, the feed and part of the top deck are in the direct field of view of the reflector. We have used a corrugated conical horn feed, which has been inherited from Jason 3 [3] and covers the 18.7 GHz, 23.8 GHz and 33.9 GHz bands. An Ortho-Mode Transducer (OMT) is placed after the horn in order to separate the two linear polarizations, which are then processed by the radiometer electronics. The corrugated horn, shown in Fig. 1(a), is fixed (non-rotating). In Fig. 1(b) one can also see the top deck, which includes the reflector, the supporting struts, and a conical baffle all around the feed-horn. The baffle was added in order to reduce interaction between reflector and top deck. Contrary to the horn, the top deck spins in order to provide a conical scan of the antenna beam footprint, similar to the mesh reflector in the SMAP mission [4]-[5].

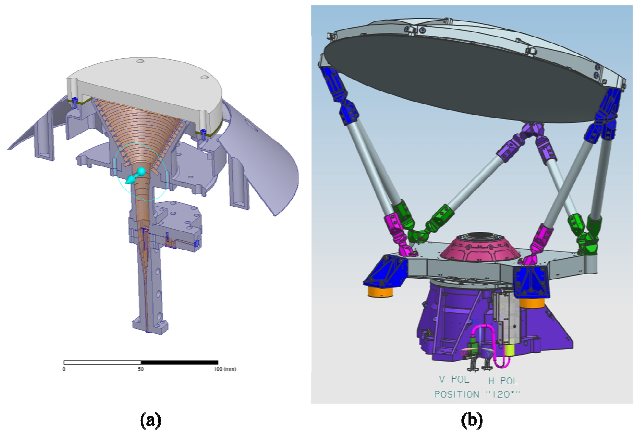

Fig. 1. (a) Detail of the corrugated conical horn, with the baffle around and covered with an EPS radome. (b) CAD Model of the COWVR instrument antenna in its 120° position including (in purple under the top deck) the Spinning Mechanism Assembly (SMA).

Bearing in mind the configuration of the instrument, we now describe the steps taken for an accurate EM modelling. First, the entire feed assembly, including the surrounding baffle and the expanded polystyrene (EPS) radome that covers the horn (Fig. 1(a)), was modeled in HFSS [6]. The calculated radiation patterns also take into account the phase delay between polarizations introduced by the OMT. In a second step, a simplified model of the instrument, which includes the top deck, the conical baffle, the struts, and the

reflector (see Fig. 2) has been introduced in GRASP [7]. A spherical wave expansion (SWE) of the HFSS radiation patterns is used as source in GRASP. Then, the multilevel fast multipole method (MLFMM) [8] add-on of GRASP is applied to obtain the total radiation pattern. The accuracy of this hybrid HFSS-GRASP model is discussed in Section IV, where a detailed comparison with measurements is shown.

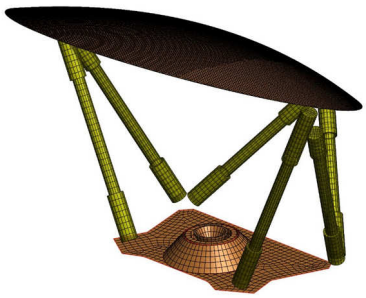

Fig. 2. Simplified RF Model used in GRASP™ to generate the calculated results.

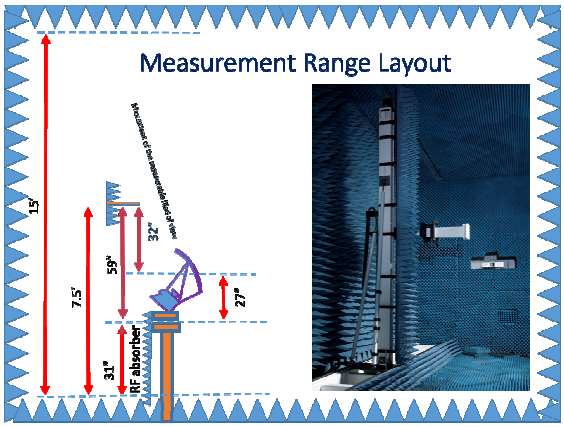

Fig. 3. Left: schematic of the COWVR instrument mounted on the pedestal. Right: picture of the NSI planar near-field range in the 60' chamber of the JPL Mesa.

III. Radiation Pattern Measurement Setup

The performance of COWVR's antenna, including the Spinning Mechanism Assembly (SMA) and the top deck assembly, was measured with the NSI planar near-field range facility in the 60 ft chamber of the JPL MESA Antenna Test Facility, shown in Fig. 3. The high gain of the antenna under test (> 40dB) motivated the choice of a planar scanner. Both the SMA and top deck assembly were mounted on a pedestal (see Fig. 4), with the main beam pointing perpendicular to the scan plane, as shown in Fig. 3. The pedestal has the capability of rotating the SMA, while the reflector remains fixed and accurately pointed at the scanner. This way, one can introduce the effect of the top deck rotation around Nadir. Using this set-up, 3 positions of the top deck (90°, 120° and 180°) have been measured. The last position was also measured with aluminum foil distributed on the top deck as in Fig. 4(b) in order to simulate the presence of Multi-Layer Insulation (MLI) thermal blankets. It is important to note that, in order to guarantee excellent accuracy, each position was correlated with metrology data to assess the actual pointing of the instrument in the range reference system.

The motivation for carrying out this measurement campaign was twofold. First, to verify the accuracy of the predictions made with the RF model described in Section II. Second, we wanted to establish whether it was possible to use the model rather than the measurements for on orbit radiometer calibration. Such point had been verified with a scaled model for the SMAP mission [5].

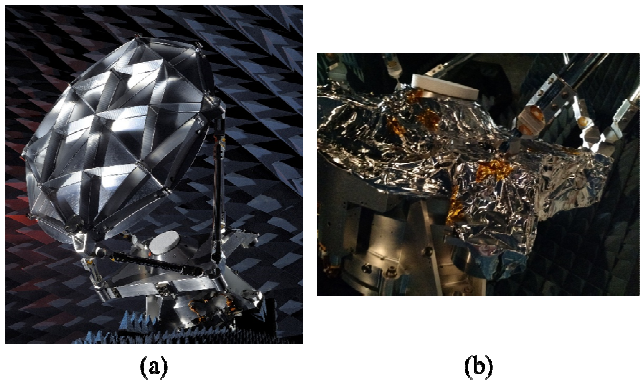

Fig. 4. (a) SMA and top deck assembly mounted on the pedestal in the 60' chamber of the JPL Mesa. (b) Detail of the top deck covered with aluminum foil to simulate the MLI thermal blankets.

IV. Comparison Between Measurements and Predictions From The RF Model

Next, we summarize the results obtained with the RF model described in Section II, and the measurements that correspond to the setup in Section III. Both simulations and measurements were carried out for all three orientations and frequency bands. However, we will only show the patterns obtained for the vertical polarization at the 180° position and 33.9 GHz, given that the conclusions drawn for this case can be extrapolated for all the other position-frequency pairs.

Fig. 5 shows in light blue and light green the simulated co-polarized (Co-Pol) and cross-polarized (Cx-Pol) components of the radiation patterns, respectively. Conversely, the dark green and dark blue lines represent the measured Co-Pol and Cx-Pol far-fields, respectively. The red and brown lines stand for the measured Co-Pol and Cx-Pol far-fields, when the top deck is covered with aluminum foil. One can appreciate a remarkably good agreement, within the line thickness, for all the Co-pol components around the main beam, both in the elevation, Fig. 5(a), and azimuth, Fig. 5(b), cuts. Only a slight difference can be appreciated in side lobes 40 dB below the peak. The agreement obtained is equally good for the Cx-Pol fields in azimuth, whereas the measured Cx-Pol in elevation is somewhat higher than the predicted one. Nonetheless, the Cx-Pol level is still more than 30 dB lower than the maximum and within the specifications. It is also important to note that adding the aluminum foil has no effect in the measurements.

In the top row of Fig. 6, one can see Elevation/Azimuth color-maps of the measured Co-Pol and Cx-Pol far fields (without the aluminum foil), while the bottom row shows the simulated Co-Pol and Cx-Pol patterns. The yellow areas are 30 dB below the peak, and all the features in the measured patterns are successfully reproduced by the RF model. In addition, we have summarized in Table 1 the measured and computed directivities for the 180° position, at 18.7 GHz, 23.8 GHz and 33.9 GHz and for both polarizations. The measured H-Pol and V-Pol directivities are within 0.1dB of the calculated values.

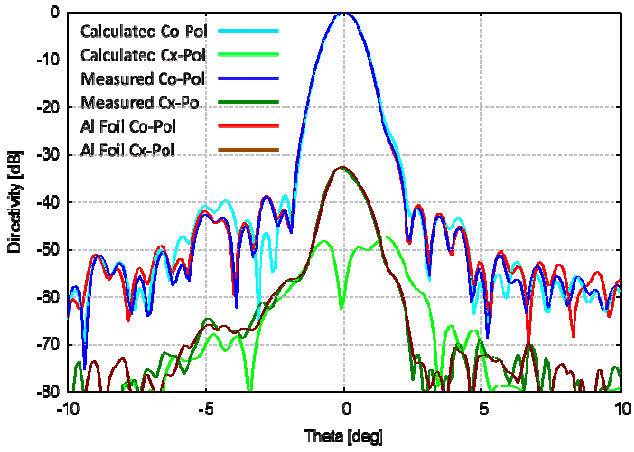

(a)

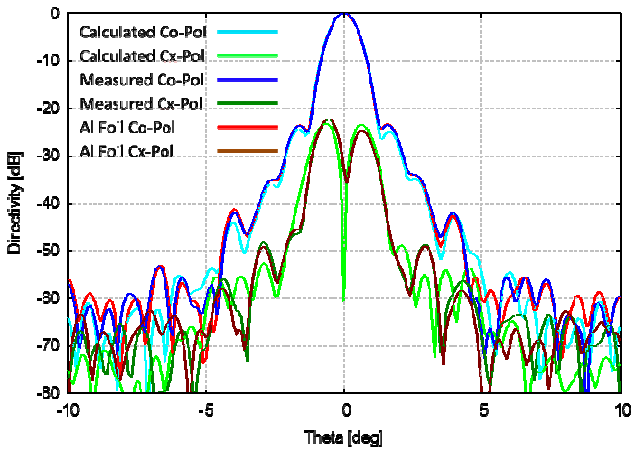

(b)

Fig. 5. Calculated and measured far-field radiation patterns for the vertical polarization, and the 180 SMA position at 33.9 GHz: (a) elevation cut and (b) azimuth cut.

Finally, the accuracy of the pointing has been evaluated as well. The complete set of results are not shown here, however we have verified that pointing is always within a few milli-degrees of the calculated values in all frequency bands. Only the higher band presents more variability (just a few tens of milli-degrees) due to small mechanical instability during the measurements. The results in this section confirm the high level of accuracy of the RF Models, which opens the possibility of using calculated results for on orbit radiometer calibration.

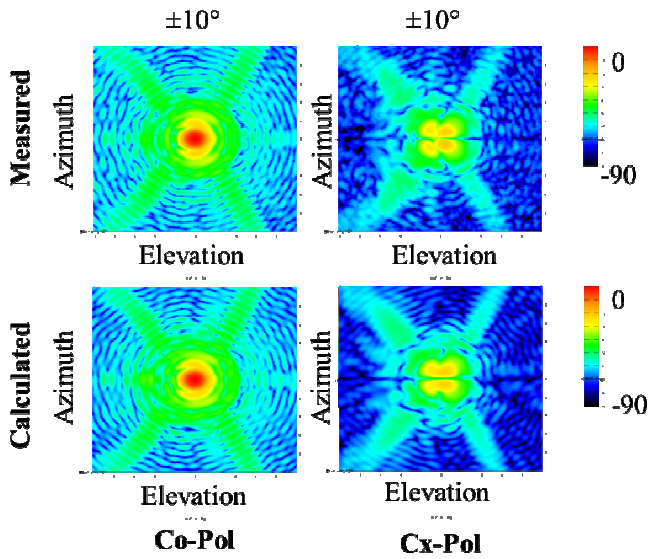

Fig. 6. Comparison between measured (top) and calculated (bottom) 2D radiation patterns in Elevation/Azimuth format at 33.9 GHz for Co-Pol and Cx-Pol horizontal polarizations.

Table 1. Measured and simulated directivities.

	Frequency	Measured Directivity	Calculated Directivity
V-Pol	18.70 GHz	40.61 dB	40.56 dB
	23.80 GHz	42.69 dB	42.67 dB
	33.90 GHz	45.59 dB	45.50 dB
H-Pol	18.7 GHz	40.63 dB	40.55 dB
	23.80	42.70 dB	42.66 dB
	33.90 GHz	45.57 dB	45.55 dB

V. Improved RF Model

A larger RF model, shown in Fig. 7 has been developed in order to assess the impact of solar panels protruding into the field of view of the reflector, once the instrument is mounted on the spacecraft. The structure has been simulated for a full rotation of the SMA in 20° steps, although only two different positions are shown in the top row of Fig. 8, left: 0° and right: 120°. The middle row shows a 2D plot of the Co-Pol far-fields for the vertically polarized input, whereas the bottom row shows the Cx-Pol far-fields. The simulation frequency for the plots in Fig. 8 is 33.9 GHz. If one compares the plots in the middle and bottom rows, one can see that the Co-Pol side-lobes plots, and the Cx-Pol (in yellow) rotate following the rotation of the SMA. Nevertheless, such rotation can be appreciated only for power levels that are 30 dB below the peak and for the

higher frequency. This effect disappears at 18.7 and 23.8 GHz.

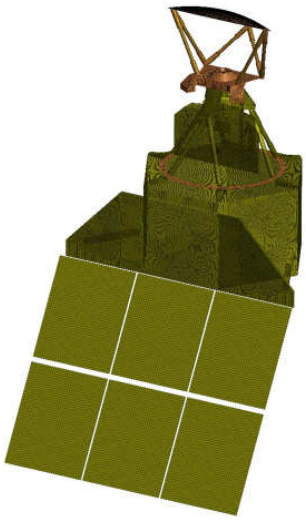

Fig. 7. Improved GRASP model including the spacecraft bus and the deployed solar panels.

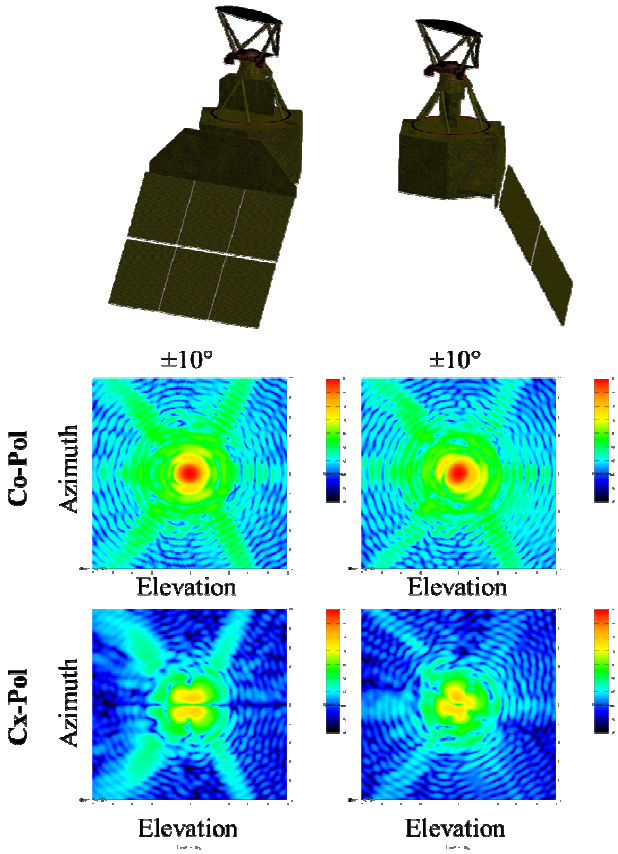

Fig. 8. Top row: GRASP model of the SMA on the spacecraft bus with solar panels deployed for the 0° (left) and 120° (right) positions. Middle row: Co-Pol far-fields for the 0° (left) and 120° (right) positions, vertically polarized pattern. Bottom row: X-Pol far-fields for the 0° (left) and 120° (right) positions, vertically polarized pattern.

VI. Conclusions

The presented results confirm the high level of accuracy already demonstrated by the latest RF Models. Overall, we have demonstrated a very good agreement over a very large dynamic range (60 dB). All features of the radiation patterns were predicted with extreme accuracy. Directivities were measured to within 0.1 dB of predicted values. Pointing also showed good agreement with predicted values, even though there was a larger variability at the higher band due to small mechanical instability in the measured data. Thanks to results like those presented in this paper, flight projects can now rely on RF models when measurements are too expensive or too complex to perform.

Acknowledgment

The research was carried out at the Jet Propulsion Laboratory, California Institute of Technology, under a contract with the National Aeronautics and Space Administration. © 2016 California Institute of Technology. Government sponsorship acknowledged.

References

[1] P. W. Gaiser, K. M. St Germain, E. M. Twarog, G. A. Poe, W. Purdy, D. Richardson, W. Grossman, W. L. Jones, D. Spencer, G. Golba, J. Cleveland, L. Choy, R. M. Bevilacqua, P. S. Chang, "The WindSat Spaceborne Polarimetric Microwave Radiometer: Sensor Description and Early Orbit Performance," *IEEE Trans. Geosci. Remote Sens.*, vol.42, no.11, pp.2347-2361, Nov. 2004.

[2] S. T. Brown, P. Focardi, A. Kitiyakara, F. Maiwald, O. Montes, S. Padmanabhan, R. Redick, D. Russell, and J. Wincentsen, "The Compact Ocean Wind Vector Radiometer: A New Class of Low-Cost Conically Scanning Satellite Microwave Radiometer System", 94th American Meteorological Society Annual Meeting, Atlata GA, Feb. 2-6, 2014.

[3] F. Maiwald et al., "Reliable and Stable Radiometers for Jason-3," *IEEE J. Sel. Topics Appl. Earth Observ. in Remote Sens.*, vol. 9, no. 6, pp. 2754-2762, June 2016.

[4] P. Focardi, P. R. Brown, and Y. Rahmat-Samii, "Deployable Mesh Reflector Antennas for Space Applications: RF Characterizations", in *Space Antenna Handbook*, W. A. Imbriale, S. Gao and L. Boccia Eds. Chichester, UK, John Wiley & Sons, 2012.

[5] P. Focardi, P. R. Brown, J. D. Vacchione and J. A. Harrell, "SMAP: Performance verification and testing of a challenging instrument antenna," *Proc. 9th Eur. Conf. Antennas Propag. (EuCAP)*, Lisbon, 2015, pp. 1-3.

[6] ANSYS Inc., "HFSS, Version 15," Pittsburgh, PA, 2015.

[7] Ticra, "GRASP,Version 10.5" Copenhagen, Denmark, 2015.

[8] O. Borries, P. Meincke, E. Jørgensen and P. C. Hansen, "Multilevel Fast Multipole Method for Higher Order Discretizations," *IEEE Trans. Antennas Propag.*, vol. 62, no. 9, pp. 4695-4705, Sept. 2014.